

Sources of negative differential resistance in electric nanotransport

Ioan Bâldea* and Horst Köppel

Theoretische Chemie, Universität Heidelberg,

Im Neuenheimer Feld 229, D-69120 Heidelberg, Germany

Abstract

A negative differential resistance (NDR) in the nanotransport is often ascribed to electron correlations. We present a simple example which demonstrates that finite electrode bandwidths and energy dependent electrode density of states are responsible for significant NDR effects, which occur even in uncorrelated nanotransport. Therefore, special care is needed in assessing the contribution of electron correlations to the NDR.

PACS numbers: 73.63.-b, 85.35.Be, 85.35.Gv, 85.65.+h

The fact that the current-voltage (I - V) characteristics of the dc-transport can exhibit a negative differential resistance (NDR) in systems described within a single-particle picture, and is not necessarily related to electron correlations is well known in semiconductor physics (see, e. g., Ref. 1). However, in the nanophysics community one hears every one and then that the NDR in the I - V curve is an effect of (presumably strong) electron correlations. In fact, some calculations performed on simple but nontrivial models of correlated electrons, like the interacting resonant level model, found no NDR effect far away from resonance,^{2,3} while other calculations revealed a more⁴ or less^{5,6} pronounced NDR effect at resonance. At the end of this note, we shall return to the NDR effect within the interacting resonant model. Beforehand — and this is the main aim of the present work — we want to emphasize that other, more common sources of the NDR are relevant for nanotransport as well. Therefore, special care is needed if one attempts to ascribe the NDR to electron correlations.

The naive “argument” behind the confusion that the NDR is an electron correlation effect seems to be the following. Within the Landauer approach of the transport in uncorrelated systems, the current resulting from the imbalance between the source and drain chemical potentials $\mu_S = \varepsilon_F + eV_{sd}/2$ and $\mu_D = \varepsilon_F - eV_{sd}/2$ is expressed as an integral of the transmission coefficient $T(\varepsilon)$ over energies from $\varepsilon = \mu_D$ to $\varepsilon = \mu_S$. An NDR cannot occur because the current monotonically increases, since the integrand is positive [$T(\varepsilon) \geq 0$] and the integration range increases as the voltage V_{sd} becomes higher.

To illustrate that this is not the case, let us consider a two-terminal setup (Fig. 1), consisting of a nanosystem [quantum dot(s) or molecule(s)] linked to two semi-infinite electrodes (source and drain) at zero temperature. For simplicity, their bandwidth $4t$ as well as their coupling to (say,) the dot τ will be supposed to be identical. By gradually rising the source-drain voltage V_{sd} starting from $V_{sd} = 0$, the drain current I_{sd} will first progressively increase because the energy window ΔE of the (elastic) electron tunneling processes allowed by Pauli’s principle becomes broader (Fig. 1a). However, further increasing V_{sd} beyond half of the electrode bandwidth ($eV_{sd}^* \equiv 2t$) will diminish this energy window (Fig. 1b), and this will be accompanied by a current reduction, which becomes more and more pronounced as the electrode band edge is approach. For $eV_{sd} \geq 4t$, elastic tunneling is no longer possible, and the current is completely blocked ($I_{sd} = 0$). This fact that the current I_{sd} should diminish as V_{sd} exceeds V_{sd}^* and is completely suppressed above the band edge ($4t$) applies for a general two-terminal setup for a sufficiently weak hybridization $\Gamma_0 \equiv 2\tau^2/t$.

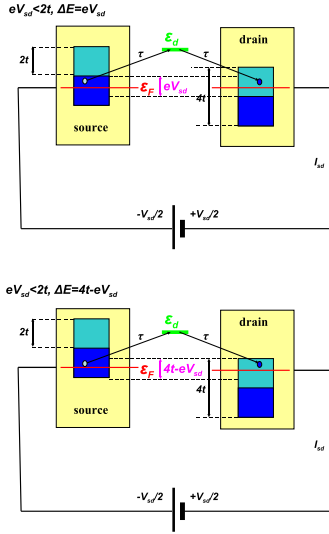


FIG. 1: (Color online) Schematical representation of a typical two-terminal setup. By gradually increasing the source-drain voltage V_{sd} the energy window ΔE of the allowed elastic tunneling processes increases for $eV_{sd} < 2t$ (panel a), but beyond the point $eV_{sd} = 2t$ (electrode half-bandwidth) it decreases (panel b). Elastic tunneling cannot occur for $eV_{sd} \geq 4t$.

To make the analysis more specific, let us consider a simple point contact (noninteracting resonant level) model, wherein the nanosystem consists of a single nondegenerate level of energy ε_g linked to one-dimensional semi-infinite electrodes. The second-quantized Hamiltonian reads

$$\begin{aligned}
H = & -t \sum_{l \leq -1} (c_l^\dagger c_{l-1} + h.c.) + \mu_S \sum_{l \leq -1} c_l^\dagger c_l \\
& -t \sum_{l \geq 1} (c_l^\dagger c_{l+1} + h.c.) + \mu_D \sum_{l \geq 1} c_l^\dagger c_l \\
& + \varepsilon_g c_0^\dagger c_0 - \tau (c_{-1}^\dagger c_0 + c_1^\dagger c_0 + h.c.) .
\end{aligned} \tag{1}$$

As usual, we set $t = 1$ and $\varepsilon_F = 0$. We shall consider $\varepsilon_g \geq 0$ (i. e, LUMO- or n-type conduction) for all the numerical results presented below (as also done in Fig. 1), but note that the values $+\varepsilon_g$ and $-\varepsilon_g$ are equivalent because model (1) possesses particle-hole symmetry. The electrode-dot coupling τ yields well known expressions of the embedding self-energies $\Sigma_x(\varepsilon) = \Delta_x(\varepsilon) - i\Gamma_x(\varepsilon)/2$ ($x = S, D$), where^{7,8}

$$\begin{aligned}
\Delta_x(\varepsilon) &= \Delta(\varepsilon - \mu_x); \Gamma_x(\varepsilon) = \Gamma(\varepsilon - \mu_x); \\
\Delta(\varepsilon) &= \frac{\tau^2 \varepsilon}{2t^2}; \Gamma(\varepsilon) = \frac{\tau^2}{t^2} \sqrt{4t^2 - \varepsilon^2} \theta(2t - |\varepsilon|).
\end{aligned} \tag{2}$$

They can be plugged into the Dyson equation

$$G^{-1}(\varepsilon) = \varepsilon - \varepsilon_g - \Sigma_S(\varepsilon) - \Sigma_D(\varepsilon) \quad (3)$$

to obtain the retarded Green function $G(\varepsilon)$ of the embedded dot. With the aid of the latter, the electric current can be expressed as (electron spin is disregarded)

$$\begin{aligned} I_{sd} &= \frac{e}{\hbar} \int_{\mu_D}^{\mu_S} d\varepsilon T(\varepsilon) = \frac{e}{\hbar} \int_{\mu_D}^{\mu_S} d\varepsilon \Gamma_S(\varepsilon) \Gamma_D(\varepsilon) |G(\varepsilon)|^2, \\ &= \frac{e}{\hbar} \int_{\mu_D}^{\mu_S} d\varepsilon \frac{\Gamma_D(\varepsilon) \Gamma_S(\varepsilon)}{[\varepsilon - \varepsilon_g - \overline{\Delta}(\varepsilon)]^2 + \overline{\Gamma}(\varepsilon)^2/4}, \end{aligned} \quad (4)$$

where $\overline{\Gamma}(\varepsilon) \equiv \Gamma_D(\varepsilon) + \Gamma_S(\varepsilon)$ and $\overline{\Delta}(\varepsilon) \equiv \Delta_D(\varepsilon) + \Delta_S(\varepsilon)$.

I - V characteristics computed exactly by means of Eq. (4) at resonance ($\varepsilon_g = 0$) are depicted by the thick lines in Fig. 2. These curves quantitatively show that, indeed, the current is suppressed as the voltage approaches the bandwidth and disappears beyond $eV_{sd} > 4t$. Away from resonance ($\varepsilon_g \neq 0$), a new aspect is visible in Fig. 3a. The current vanishes even below the bandwidth $4t$. Practically, the suppression is complete at $V_{sd} = 4t - \varepsilon_g$; beyond this value, the I - V curves only exhibit negligible tails of widths $\sim \Gamma_0 = 2\tau^2/t$. On the other side, the exact I - V characteristics of Figs. 2 and 3a reveal that the current decreases well before reaching the value $V_{sd}^* = 2t/e$, which one could expect from the inspection of Fig. 1. This demonstrates that the finite bandwidth effect discussed above is only *one* reason why the NDR should occur.

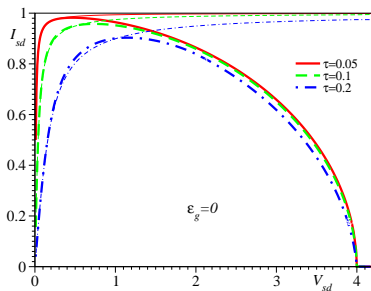


FIG. 2: (Color online) I - V curves at resonance ($\varepsilon_g = \varepsilon_F = 0$) for $\tau = 0.05; 0.1; 0.2$ computed exactly (thick lines) and within approximation (i) described in the text (thin lines). Current I_{sd} in units $I_{sd}^s = \pi e \Gamma_0 / h$.

Significant physical insight can be gained by examining three limits of Eq. (4):

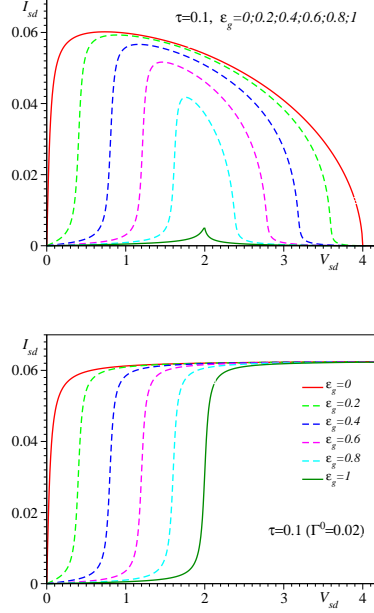


FIG. 3: (Color online) I - V curves out of resonance for $\tau = 0.1$ ($\Gamma_0 = 0.02$) computed exactly (panel a) and within approximation (i) described in the text (panel b) for $\epsilon_g = 0; 0.2; 0.4; 0.6; 0.8; 1$ (values increasing downwards). Current in units et/h .

(i) One can approximate the embedding energies by their values at $\varepsilon = \mu_x$, i. e., $\Sigma_{S,D} \simeq -i\Gamma_0/2$, in the *whole* integration range, which means to simply ignore the presence of the Heaviside θ functions in Eq. (2). One then gets the current

$$I_{sd}^{low} = \frac{e\Gamma_0}{h} \left(\arctan \frac{eV - 2\varepsilon_g}{2\Gamma_0} + \arctan \frac{eV + 2\varepsilon_g}{2\Gamma_0} \right). \quad (5)$$

As this amounts to assume that the electrode bandwidth is the largest energy scale (more precisely, for $V_{sd}, \varepsilon_g, \tau \ll t$), Eq. (5) is usually referred to as the wide band limit.

(ii) Next, one can compute the current using the electrode density of states (DOS) Γ_x for $\varepsilon = \mu_x$, but unlike above, considering the Heaviside θ functions in Eq. (2)

$$I_{sd}^{fb} = \frac{e\Gamma_0}{h(1 - \tau^2/t^2)} \left(\arctan \frac{\Lambda_+}{2\Gamma_0} + \arctan \frac{\Lambda_-}{2\Gamma_0} \right), \quad (6)$$

where $\Lambda_{\pm} \equiv [\min(eV_{sd}, 4t - eV_{sd}) \pm 2\varepsilon_g] \times (1 - \tau^2/t^2)$. Similar to the previous approximation, the electrode DOS is assumed constant, but the fact that the electrode bandwidths are *finite* (i. e., the main ingredient of the physical analysis based on Fig. 1) is taken into account by this approximation.

(iii) Because the main contribution to the integral in Eq. (4) comes from the pole of the Green function of the isolated dot, one can use the embedding energies calculated at $\varepsilon = \varepsilon_g$.

In fact, this approximation yields very accurate I - V curves, which are not shown because they could be hardly distinguished from the exact curves within the drawing accuracy of Figs. 2, 3a, 4, and 5. More instructive is however to furthermore assume that the voltage V_{sd} is sufficiently high and extend the integration in Eq. (4) from $-\infty$ to $+\infty$. The result is

$$I_{sd}^{high} = \frac{e}{\hbar} \frac{\Gamma(\varepsilon_g - eV/2)\Gamma(\varepsilon_g + eV/2)}{\Gamma(\varepsilon_g - eV/2) + \Gamma(\varepsilon_g + eV/2)}. \quad (7)$$

I - V curves in the limit (i) are depicted in Figs. 2 (thin lines), 3b, and 4. They show a monotonically increasing current, which exhibits a step at $eV_{sd} \simeq 2\varepsilon_g$ of width δV_{sd} increasing with τ and rapidly saturates at an ε_g -independent value $I_{sd}^s = \pi e\Gamma_0/h$. Such curves are usually shown in textbooks, and this feeds the lore of the absent NDR in uncorrelated systems.

What is wrong with the naive argument against the NDR in uncorrelated systems is that the transmission is *not* independent of V_{sd} . The V_{sd} -dependence enters via the electrode densities of states $\Gamma_{S,D}$ [cf. Eq. (2)].

On one side, this dependence is considered by the step functions θ entering Eq. (2), which diminish the energy window of allowed tunneling processes (cf. Fig. 1). Approximation (ii) that accounts for this yields two qualitatively correct results: an NDR beyond V_{sd}^* , where the predicted I - V characteristics exhibits a cusp (cf. Fig. 5) and a vanishing current for $eV_{sd} \geq 4t$. Quantitatively, the NDR onset (at $V_{sd} = V_{sd}^*$) is unsatisfactory; compare these approximate curves (label *fb*) with the exact ones in Figs. 4 and 5. The NDR occurs well below the point predicted by this approximation.

On the other side, not only the step functions θ , but also the ε -dependence of the electrode DOS [expressed by the square roots in Eq. (2)] is important. It is this fact that makes the finite bandwidth argument incomplete. The ε -dependence of $\Gamma_{S,D}$ is accounted for within approximation (iii). The comparison with the exact curves (Fig. 4) reveals an excellent agreement at sufficiently higher voltages (as assumed within this approximation) and demonstrates that, to describe quantitatively the NDR, one has to consider both the allowed energy window, which is finite, and the energy dependence of the electrode DOS.

In Fig. 4, we present exact I - V characteristics from Eq. (4) along with those computed within the three aforementioned approximations, Eqs. (5), (6), and (7). As visible there, approximation (i) is accurate for lower voltages, while approximation (iii) is accurate for higher voltages. The crossover occurs at a voltage V_{sd}^{NDR} , which can be identified with the

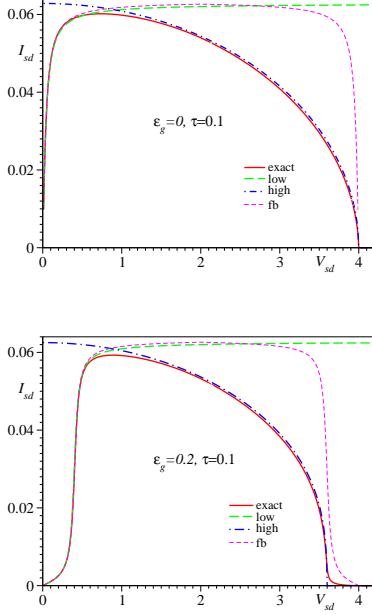


FIG. 4: (Color online) I - V curves for $\tau = 0.1$ ($\Gamma_0 = 0.02$) computed exactly and within the approximations described in the text at resonance $\varepsilon_d = 0$ (panel a) and out of resonance, $\varepsilon_d = 0.2$ (panel b). Current in units et/h . Labels as in Eqs. (5), (6), and (7).

NDR onset. This value can be obtained by equating

$$I_{sd}^{low}(V_{sd}^{NDR}) = I_{sd}^{high}(V_{sd}^{NDR}). \quad (8)$$

Curves for V_{sd}^{NDR} are presented in Fig. 6. They show that for situations not very far away from resonance and sufficiently weak electrode-dot couplings τ , V_{sd}^{NDR} is considerably smaller than the value $eV_{sd}^* = 2t$ expected from the finite bandwidth argument. The significant departure of the NDR onset predicted exactly and within approximation (ii) is also clearly depicted in Fig. 5. For smaller τ 's one can deduce an analytical estimate

$$V_{sd}^{NDR} \simeq 2\varepsilon_g + c(t\tau^2)^{1/3}, \quad (9)$$

where c is a numerical factor ($c \simeq 4$).

Interesting for nanotransport are the electron level(s) not too misaligned with electrode's Fermi level; otherwise, as illustrated by the curve for $\varepsilon_g = t$ in Fig. 3a, the current is very small. Therefore, the results on V_{sd}^{NDR} expressed by Eq. (9) and Fig. 6 are perhaps the most relevant ones from an experimental perspective. They indicate that an NDR could be observed in the experimental I - V data at reasonably low voltages. For this, V_{sd} needs not

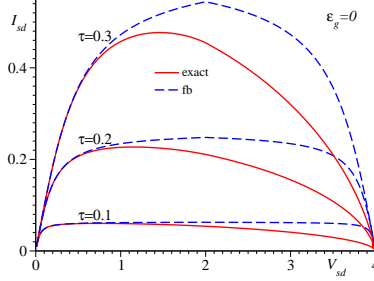


FIG. 5: (Color online) I - V curves on resonance ($\varepsilon_g = 0$) for the three electrode-dot couplings τ specified in the inset computed exactly and within approximation (ii) described in the text (label fb). Notice that the latter exhibit a cusp at $eV_{sd} = 2t$ that marks the NDR onset in this approximation, which can be substantially higher than the exact NDR onset.

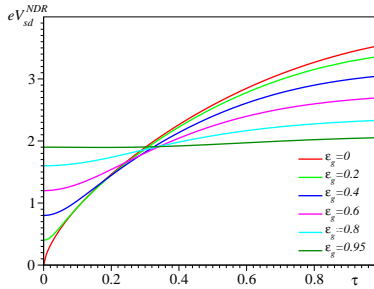


FIG. 6: (Color online) Curves for the NDR onset voltage V_{sd}^{NDR} computed from Eq. (8) for several level energies ε_g . Notice that for smaller electrode-dot couplings τ and not too far away from resonance V_{sd}^{NDR} is significantly smaller than 2 (half of electrode's bandwidth).

represent a substantial fraction of the electrode bandwidth $4t$ and can be much than the value V_{sd}^* predicted by assuming a constant electrode DOS. This aspect is very important especially for (metallic) electrodes characterized by a wide bandwidth, because otherwise a too high voltage could damage the nanoprobe before an NDR effect could be observed. Again quite relevant for experiments, the NDR onset can be controlled by tuning level's energy ε_g with the aid of a gate potential. Such methods of gatings, which were routinely employed for artificial nanosystems more than one decade ago⁹, were also successfully applied recently in molecular transport.¹⁰

In the above analysis, we have presented results perhaps for the simplest uncorrelated nanosystem, which possesses a single “active” level of energy ε_g . In the real world, this could correspond to the highest occupied electron level of a quantum dot. The employed model

could also describe the molecular transport either through the highest occupied molecular orbital (HOMO, p-type conduction, as in the beautiful recent experiment of Ref. 10) or through the lowest unoccupied molecular orbital (LUMO, n-type conduction, as schematically depicted in Fig. 1) of a weakly correlated molecule, depending on whether the former or the latter is closer to the electrode Fermi energy. The present analysis can be extended without difficulty to nanosystems/molecules with several “active” electron levels. As long as these levels $\varepsilon_{g1}, \varepsilon_{g2}, \dots$ are well separated energetically and the hybridization is weak enough (a different situation can also be encountered, see Ref. 11) they manifest themselves as current steps at the voltages $eV_{sd} \approx 2\varepsilon_{g1}, 2\varepsilon_{g2}, \dots$. However, even in this case the finite electrode bandwidth and the energy dependence of the electrode DOS remain possible important sources of an NDR.

Similar to other situations encountered in nanotransport,^{12,13} we believe that the results for uncorrelated systems are instructive and could also be useful to correctly interpret the nanotransport in correlated systems. In the present concrete case, they could help to unravel the physical origin of the NDR. In the light of the present analysis, it is plausible to ascribe an NDR as an electron correlation effect in cases where the NDR was found within calculations to a correlated nanosystem carried out within the wide band limit. This is, e. g., the case of Refs. 6 and 5, where a weaker NDR effect was obtained at resonance at stronger Coulomb contact interactions. As suggested by Fig. 3, the farther away from resonance, the more is the NDR onset pushed towards higher voltages ($eV_{sd}^{NDR} > 2\varepsilon_g$). The values of V_{sd} chosen in the figures shown in Ref. 3 do not belong to this range and the absence of an NDR could be related to this fact. Unlike the wide (infinite) band limit assumed in the aforementioned references, a discrete model of the electrodes, with a finite bandwidth $4t$, *exactly* as in Eq. (1), has been utilized for the numerical calculations of Ref. 4 at resonance. The I - V curves reported there exhibit a pronounced NDR effect. However, in view of the finite bandwidth assumed in that work, attributing this effect to electron correlations at rather high voltages should be made with special care. We believe that in order to interpret this effect reliably, one should first carefully subtract the contribution to the NDR due to the finite bandwidth and the energy dependent electrode DOS discussed above.

The financial support for this work from the Deutsche Forschungsgemeinschaft is grate-

fully acknowledged.

- * Also at National Institute for Lasers, Plasma, and Radiation Physics, ISS, POB MG-23, RO 077125, Bucharest, Romania
- ¹ W. R. Frensley, *Rev. Mod. Phys.* **63**, 215 (1991).
- ² P. Mehta and N. Andrei, *Phys. Rev. Lett.* **96**, 216802 (2006).
- ³ P. Mehta, S. Chao, and N. Andrei, *cond-mat/0703426*.
- ⁴ E. Boulat, H. Saleur, and P. Schmitteckert, *Phys. Rev. Lett.* **101**, 140601 (2008).
- ⁵ A. Nishino, T. Imamura, and N. Hatano, *Phys. Rev. Lett.* **102**, 146803 (2009).
- ⁶ B. Doyon, *Phys. Rev. Lett.* **99**, 076806 (2007).
- ⁷ C. Caroli, R. Combescot, P. Nozières, and D. Saint-James, *J. Phys. C: Solid State Physics* **4**, 916 (1971).
- ⁸ A. Nitzan, *Ann. Rev. Phys. Chem.* **52**, 681 (2001).
- ⁹ D. Goldhaber-Gordon, H. Shtrikman, D. Mahalu, D. Abusch-Magder, U. Meirav, and M. A. Kastner, *Nature* **391**, 156 (1998).
- ¹⁰ H. Song, Y. Kim, Y. Kim, Y. H. Youngsang, H. Jeong, M. A. Reed, and T. Lee, *Nature* **462**, 1039 (2009).
- ¹¹ M. C. Toroker and U. Peskin, *J. Phys. B: Atom. Molec. Opt. Phys.* **42**, 044013 (2009).
- ¹² I. Bâldea and H. Köppel, *Phys. Rev. B* **78**, 115315 (2008).
- ¹³ I. Bâldea and H. Köppel, *Phys. Rev. B* **80**, 165301 (2009).